Guo *et al. Microstructures* **2025**, *5*, 2025078
DOI: 10.20517/microstructures.2024.183

Microstructures

Research Article

Open Access

Check for updates

Manipulating stable four-electron zinc-iodine batteries via the introduction of diamine ligand sites

Qijiayi Guo[1,#], Chao Qiu[1,#], Yang Zhang[2], Jing Li[1], Zhixiang Chen[1], Fulong Li[1], Weifeng Liu[1], Xinlong Tian[1], Xiaodong Shi[1]

[1]School of Mechanical and Electrical Engineering, School of Marine Science and Engineering, School of Chemistry and Chemical Engineering, Hainan University, Haikou 570228, Hainan, China.
[2]Precision Industry Revolution Equipment Technology (Henan) Co. Ltd., Zhengzhou Research Institute for Abrasives and Grinding Co. Ltd., Zhengzhou 450007, Henan, China.
[#]These authors contributed equally to this work.

Correspondence to: Assoc. Prof. Jing Li, Assoc. Prof. Weifeng Liu and Assoc. Prof. Xiaodong Shi, School of Marine Science and Engineering, Hainan University, 58 Renmin Avenue, Meilan District, Haikou 570228, Hainan, China. E-mails: jli@hainanu.edu.cn; lwf008@163.com; shixiaodong@hainanu.edu.cn

How to cite this article: Guo, Q.; Qiu, C.; Zhang, Y.; Li, J.; Chen, Z.; Li, F.; Liu, W.; Tian, X.; Shi, X. Manipulating stable four-electron zinc-iodine batteries via the introduction of diamine ligand sites. *Microstructures* **2025**, *5*, 2025078. https://dx.doi.org/10.20517/microstructures.2024.183

Received: 27 Dec 2024 **First Decision:** 18 Feb 2025 **Revised:** 3 Mar 2025 **Accepted:** 5 Mar 2025 **Published:** 3 Jul 2025

Academic Editor: Zaiping Guo **Copy Editor:** Shu-Yuan Duan **Production Editor:** Shu-Yuan Duan

Abstract

Zinc-iodine batteries (ZIBs) are considered a promising energy storage system, but are still plagued by low energy density and rampant side reactions originating from active H_2O molecules in the liquid electrolyte. Realizing the coupled redox reactions within $I^-/I_0/I^+$ species, i.e., four-electron transfer reactions, is deemed an effective strategy for boosting the energy density of ZIBs, which is mainly blocked by the rapid hydrolysis of nucleophilic I^+ ions. To address these issues, urea with diamine ligand sites (-NH_2) was introduced into the liquid electrolyte [urea electrolyte (UE)] to achieve durable four-electron ZIBs. As demonstrated by the spectroscopic characterization results, -NH_2 groups can bundle the active H_2O molecules by reconfiguring the hydrogen bonds, and provide additional electrophilic ligand sites for I^+ ions. Based on these advantages, both the side reactions on the Zn anode and the I^+ hydrolysis reaction on the I_2@AC cathode are remarkably mitigated, and four-electron transfer is realized at low zinc salt concentrations. As a result, the optimized UE electrolyte effectively stabilizes the zinc metal anode, and endows the I_2@AC cathode with a high reversible capacity of 187.2 mAh g^{-1} after 250 cycles at 1 A g^{-1}. The disclosed intermolecular force modulation strategy in this work will offer a comprehensive perspective for the future design of liquid electrolytes for high-energy-density ZIBs.

Keywords: Zinc-iodine batteries, four electron transfer, urea, hydrolysis reaction of I^+ ions, hydrogen bonds

INTRODUCTION

The intermittency of clean energy and the non-renewability of fossil energy limit the sustainable development of society, which also promotes the evolution of energy storage devices[1,2]. Although lithium-ion batteries are widely applied in energy storage, their inherent flammability and toxicity have not yet been effectively addressed[3-5]. Compared with lithium-ion batteries, zinc-ion batteries exhibit significant advantages in terms of safety, environmental friendliness, and high ionic conductivity[6]. However, the application of zinc-ion batteries was also plagued by the issues of zinc metal corrosion, hydrogen evolution reaction (HER), and uncontrollable growth of zinc dendrites[7,8], which can be ascribed to the unstable electrolyte/electrode interface and active H_2O molecules. For instance, heterogeneous solid electrolyte interface (SEI) causes differences in ion deposition rate, leading to zinc dendrite growth, spontaneous H_2O decomposition at ~ 1.23 V, interfacial by-products, and zinc corrosion[9,10]. Electrolytes, as the main medium of ion transfer between the two electrodes and the precursor of SEI formation, are also key carriers that influence the forces between H_2O molecules. Electrolyte regulation engineering is an effective method to boost interfacial stability and modulate the activity of H_2O molecules[11,12].

Compared with other cathode materials, the multivalent state of iodine species allows zinc-iodine batteries (ZIBs) to achieve higher energy density[13]. The working mechanism of ZIBs is greatly distinct from the conventional zinc-ion batteries, which is featured with iodine redox reaction, corresponding to the solid-liquid conversion process[14]. Achieving the coupled redox reaction within $I^-/I_0/I^+$ is the key route to realizing four-electron ZIBs (4eZIBs), corresponding to a high theoretical energy density of 422 mAh/g[15]. Nevertheless, the electrophilic I^+ ions are highly susceptible to hydrolysis in aqueous electrolytes, blocking the continuous electron transfer and iodine redox reactions[15,16]. Scientifically, nucleophilic reagents with a stronger negative charge center than the OH^- group, such as cyanide, interhalogen compounds, and amines[17,18], can effectively capture the I^+ ion and enable consecutive iodine redox reaction. Additionally, most electrolytes still require high concentrations of zinc salts to limit the active H_2O molecules and realize the 4eZIBs[15,19]. The basic criterion for exciting 4eZIBs at low zinc salt concentrations is both inhibition of I^+ hydrolysis and reduction of H_2O activity. Weakening of H_2O activity can be achieved by disrupting the hydrogen bonds network between H_2O molecules or by regulating the solvation sheath, which, in essence, changes the forces between H_2O molecules[8,20]. Among the functional groups capable of inhibiting I^+ hydrolysis, the amine group is able to create typical hydrogen bonds with the hydroxyl group, blocking the hydrogen bonds between H_2O molecules[21]. Therefore, the amine group can be used as a nucleophilic site to stabilize I^+ species and weaken the intermolecular forces within H_2O molecules[22].

Herein, urea with diamine groups ($-NH_2$) serves as an additive to prepare liquid electrolyte [marked as urea electrolyte (UE)] for 4eZIBs with low concentrations of zinc salts, and the internal action mechanism by which $-NH_2$ groups in urea inhibit the H_2O activity and I^+ hydrolysis is further revealed. According to the spectroscopic characterizations and electrochemical test results, the introduction of urea effectively widens the electrochemical stable voltage window of UE, suppresses the growth of interfacial by-products, reduces the charge transfer impedance, and achieves the coupled redox reaction within $I^-/I_0/I^+$, which is beneficial to raise the specific capacity and cycling stability of ZIBs. Owing to these merits, Zn//I_2@AC batteries in UE display a high discharge capacity of 187.2 mAh g^{-1} after 250 cycles at 1 A g^{-1}.

MATERIALS AND METHODS

Raw materials

Urea (99.5%), iodine (99.99%), zinc acetate [$Zn(AC)_2{\cdot}2H_2O$, 99.99%], Zinc sulfate [$ZnSO_4{\cdot}7H_2O$, 99.995%], ultra-high capacitance porous activated carbon (AC), and iodine monochloride (ICl) were purchased from Aladdin Industrial. Conductive carbon black of Super P was sourced from Guangdong Canrd New Energy

Technology Co., Ltd., while carboxymethyl cellulose (CMC) binder was purchased from Duoduo Co., Ltd. All chemical reagents were used as received unless otherwise stated.

Preparation of cell

I_2@AC, CMC, and Super P (8:1:1, mass ratio) were used to prepare the cathode slurry. The 12 mm diameter I_2@AC coated on graphite paper was the cathode. The anode electrode was zinc foil (diameter ~ 12 mm, thick ~ 1 mm) and the separator was glass fiber membrane (diameter ~ 16 mm), and the CR2025-type coin cells were assembled in the ambient atmosphere. The 1 M $Zn(AC)_2{\cdot}2H_2O$ and 2 M $ZnSO_4{\cdot}7H_2O$ dissolved in deionized water were used as blank electrolyte (BE). The 1 M $Zn(AC)_2{\cdot}2H_2O$ and 2 M $ZnSO_4{\cdot}7H_2O$ dissolved in deionized water/urea (10/1, molar ratio) was used as UE.

Electrochemical measurements

Electrochemical measurements were conducted using 2025 coin-type cells. The electrochemical impedance spectra (EIS), linear sweep voltammetry (LSV), and cyclic voltammetry (CV) measurements were conducted on a Gamry (Interface 1010E) electrochemical workstation. The coin Zn||I_2 cells were operated within the voltage range of 0.6 ~ 1.85 V.

Materials characterizations

Fourier infrared spectroscopy (FTIR) spectra of electrolytes were recorded by FTIR spectrometer (Shimadzu Corporation, IRTRACER-100), Raman spectra of electrolytes were recorded by Raman spectrometer (Renishaw, inVia series), ^1H and ^{13}C NMR of the electrolytes were recorded on 600 MHZ NMR (Bruker, Avance NEO 600M). Contact Angle was recorded on Dataphysics (OCA25). Electrode was characterized by X-ray diffraction (XRD, Cu Kα radiation, Rigaku, Smart Lab SE). The field emission scanning electron microscope (FESEM, Thermo Fisher, Verios G4 UC) was used to analyze Zn deposition morphology. Thermogravimetric (TGA, Clarus SQBT, TL9000) experiments heated the sample in a N_2 atmosphere at a temperature range of 30-600 °C. X-ray photoelectron spectroscopy (XPS, Thermo Fisher, ESCALAB Xi+ or K-Alpha+) was used to analyze the Zn anode and I cathode after 10 cycles.

RESULTS AND DISCUSSION

The stable existence of I^+ ions is the key to realizing the four-electron transfer reaction of ZIBs, which is strongly influenced by the molecule activity and ligand environment in the electrolyte. As schematically illustrated in Figure 1A, ICl can be rapidly decomposed in the deionized water to generate a black precipitate of I_2 species through the following hydrolysis reaction ($5ICl + 3H_2O \rightarrow HIO_3 + 5HCl + 2I_2\downarrow$)[23]. In sharp contrast, ICl can maintain chemical stability in the urea solution of UH3 and UH10 (molar ratio: urea/H_2O = x/1, accordingly marked as UHx), demonstrating the effective inhibition of I^+ hydrolysis reaction through the introduction of urea component with double -NH_2 group. This situation can also be verified using ultraviolet-visible spectroscopy. It can be found that the absorption peak of I^+ (~ 445nm) appears in the urea solution for ICl, while in H_2O, the obvious absorption peaks of I_3^- (~ 355 nm) and I_2 (~ 450 nm) [Supplementary Figure 1][24]. Figure 1B, Supplementary Figure 2 compared the Fourier transform infrared (FT-IR) spectra of UE, BE, and urea solution, and the redshifts of -OH and -NH_2 groups indicate that the molecule ligands generated between urea and H_2O disrupt the initial hydrogen bonds within H_2O-H_2O interaction[25]. As further verified by the Raman spectra of UE, BE, and UH10 [Figure 1C and Supplementary Figure 3], the O-H stretching vibration of H_2O exhibits three peaks within 3,100 ~ 3,700 cm^{-1}, including "network water (NW)" (3,224 cm^{-1}), "intermediate water (IW)" (3,378 cm^{-1}), and "multimer water (MW)" (3,493 cm^{-1})[26]. With the addition of urea, the NW/IW rich BE is converted to an IW rich UE, manifesting the disruption and reorganization of hydrogen bonds within H_2O-H_2O, *i.e.*, O-H…O bonds are accordingly converted into O-H…N, N-H…O and N-H…N bonds. Meanwhile, the redshift of C=O (urea) in the Raman spectra of UE can be attributed to the combination of solvation effect

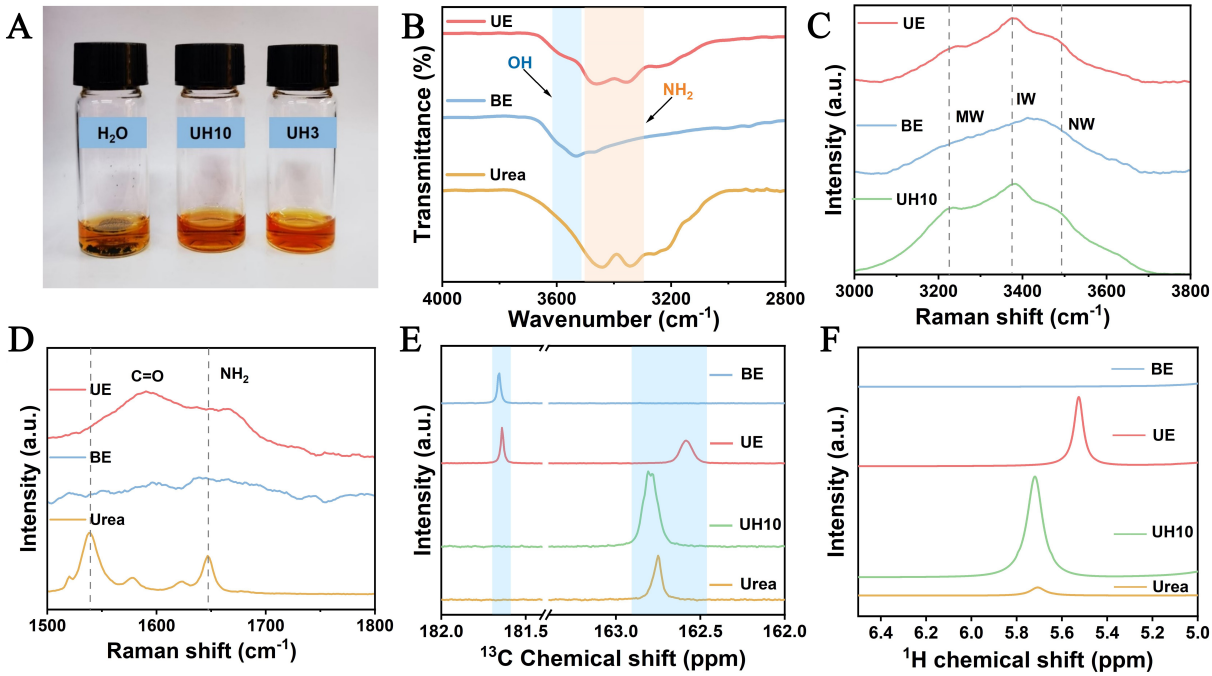

Figure 1. (A) Dissolution and hydrolysis test of ICl in different component solvents (H_2O, UH10, UH3); (B) FT-IR spectra of urea, UE and BE solutions; (C) Raman spectra of UH10, UE and BE solutions; (D) Raman spectra of urea, UE and BE solutions; (E) ^{13}C and (F) ^{1}H NMR spectra of urea, UH10, UE and BE solutions. ICl: Iodine monochloride; urea/H_2O; FT-IR: Fourier transform infrared; UE: urea electrolyte; BE: blank electrolyte; NMR: nuclear magnetic resonance.

and hydrogen bonds [Figure 1D][25,27]. Additionally, the coordination environment of BE, UE, UH10, and urea solution was further characterized by the ^{13}C and ^{1}H nuclear magnetic resonance (NMR) spectra [Figure 1E and F]. As a result, the upfield shift of COO^- groups reflects that solute anions are crowded into the solvation shell, while the upfield shift of C=O (urea) implies that urea molecules are also crowded into the solvation shell, suggesting partial H_2O molecules are excluded from the solvation shell[28]. Similarly, the upfield shift in the ^{1}H spectra can also be ascribed to the synergistic effect of solvation structure and hydrogen bonds.

The positive effect of hydrogen bonds reconfiguration on the zinc metal anode was evaluated by the linear sweep voltammetry curves of Zn//stainless steel asymmetric cells to determine the electrochemical stable voltage window of different electrolytes, which is always limited by the HER and oxygen evolution reaction (OER). As clearly demonstrated by the oxygen evolution curves [Figure 2A] and hydrogen evolution curves [Figure 2B], the reactivity of H_2O molecules in UE is effectively suppressed and the energy barriers for HER and OER are accordingly boosted, which can be attributed to the configuration change between urea and H_2O molecules through hydrogen bonds, and beneficial for the corrosion-free zinc metal anode[29,30]. Urea inevitably brings about its own self-corrosion effect at the same time. The Tafel plot Supplementary Figure 4 clearly shows the magnitudes of the corrosion currents in the 2 M $ZnSO_4$ electrolyte and the electrolyte with urea added. To alleviate its self-corrosion effect, we added zinc acetate to UE, which significantly reduced the corrosion current. As expected, compared to the Zn anode after certain cycles in BE, no significant by-products can be detected in the XRD pattern of the Zn anode in UE [Figure 2C], suggesting the inhibited side reactions on the surface of the Zn anode. Figure 2D and E, Supplementary Figure 5 contrast the micro-morphology of the Zn anode after certain cycles in different electrolytes, which helped to reflect the reversibility of zinc deposition/stripping behavior. Notably, the dense and smooth surface of the Zn anode

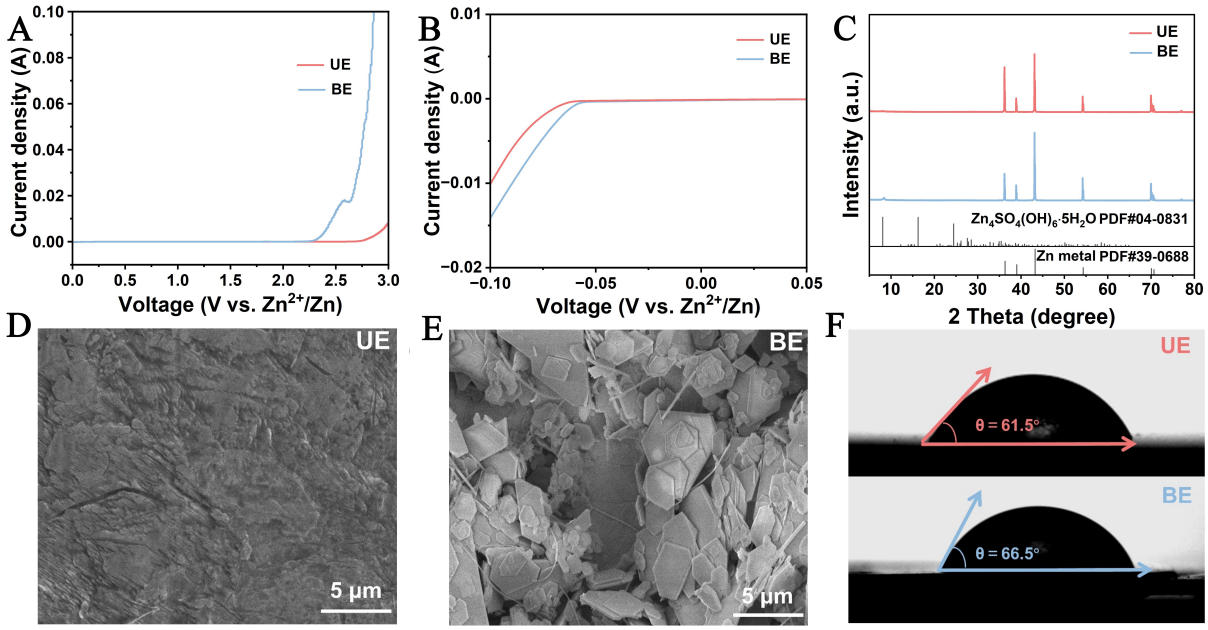

Figure 2. (A) Oxygen evolution curves and (B) hydrogen evolution curves of Zn//stainless steel asymmetric cells based on the linear sweep voltammetry test at a scan rate of 0.5 mV s^{-1}; (C) XRD patterns of Zn anode after 10 cycles in UE and BE; SEM images of Zn anode after 50 cycles in (D) UE and (E) BE; (F) Contact angles of UE and BE on the surface of Zn anode. XRD: X-ray diffraction; UE: urea electrolyte; BE: blank electrolyte; SEM: scanning electron microscope.

in UE manifests the homogeneous zinc deposition behavior with negligible by-products [Figure 2D]. On the contrary, chaotic mossy precipitates can be obviously found on the surface of the Zn anode in BE [Figure 2E], which can be ascribed to the heterogeneous zinc deposition behavior and continuous side reactions during the cycling process, always resulting in low zinc utilization and obstruction of Zn^{2+} ion deposition path[31,32]. At the same time, through the cycling of the Zn//Zn symmetric cell, the gap in excellent chemical and mechanical stabilities between the UE electrolyte and BE was further demonstrate [Supplementary Figure 6][33,34]. The UE can be cycled for at least 150 h in long-term cycling, while the battery with a rapid short circuit in the BE electrolyte was cycled for less than 70 h only. Supplementary Figure 7 clearly shows the difference in Coulombic efficiencies between UE and BE through the Zn//Cu cells, which further proves the promoting effect of urea on the uniformity of zinc deposition[35]. In addition, the contact angle was further tested to judge the affinity and wettability of different liquid electrolytes on the surface of the Zn anode [Figure 2F][36]. Owing to the differences in electrolyte components, the contact angle of UE on the Zn anode is 61.5°, slightly smaller than that in BE (65.5°), which contributes to promoting the interface stability and sufficient reaction between the Zn anode and liquid electrolyte.

XPS was conducted to qualitatively analyze the influences of different electrolytes on the interfacial by-products of Zn anode [Figure 3, Supplementary Figures 8-10]. For the high-resolution Zn 2p spectra, the relative areas of the Zn-O and Zn regions well reflect the degree of surface by-products and zinc corrosion [Figure 3A]. Consequently, compared to the partition result of the Zn anode in BE [Figure 3B], the smaller Zn-O region and the larger Zn region in UE demonstrate the effective inhibition of side reactions and zinc corrosion[9]. Meanwhile, the presence of the Zn-N region can be mainly derived from the electrochemical decomposition of urea, testifying urea is involved in the formation of SEI on the surface of the Zn anode[37,38]. Additionally, the larger area of ZnS region in high-resolution S 2p spectra [Figure 3C and D] and the larger area of O-Zn region in high-resolution O 1s spectra [Figure 3E and F] further verify the severe interfacial side reactions of Zn anode in BE, which is not conducive to the chemical stability of zinc metal[39].

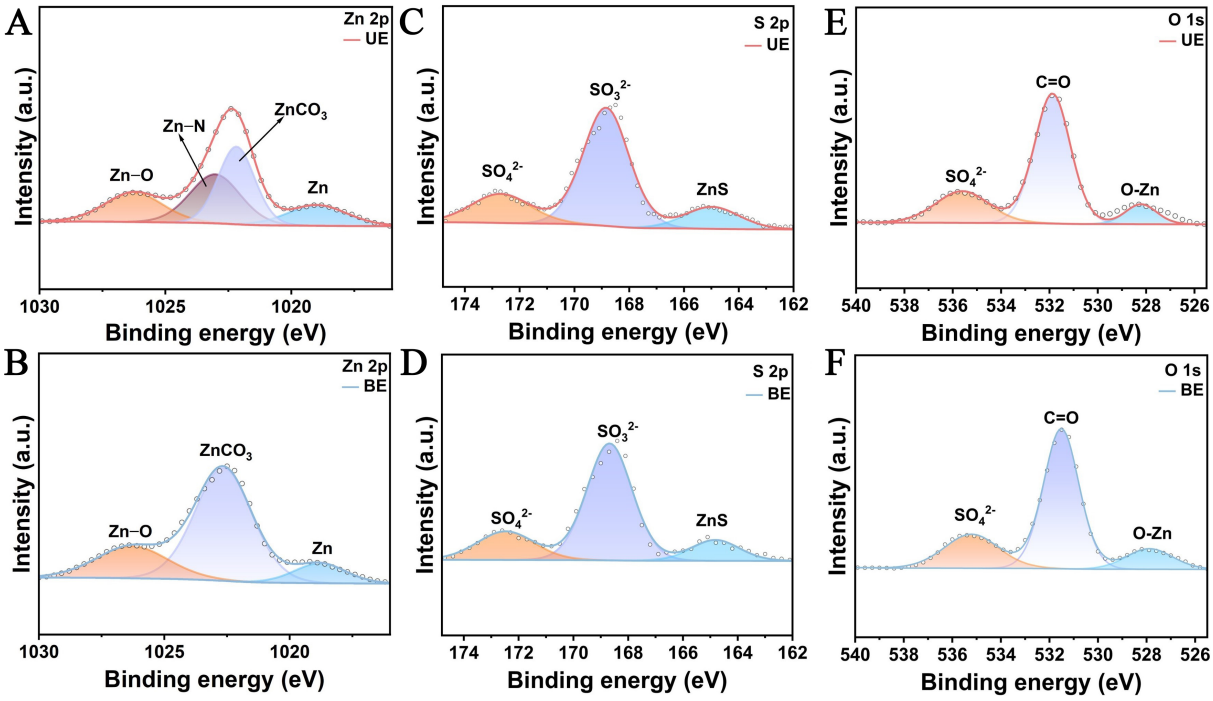

Figure 3. High-resolution Zn 2p spectra of Zn anode in (A) UE and (B) BE after 10 cycles; High-resolution S 2p spectra of Zn anode in (C) UE and (D) BE after 10 cycles; High-resolution O 1s spectra of Zn anode in (E) UE and (F) BE after 10 cycles. UE: Urea electrolyte; BE: blank electrolyte.

Supplementary Figure 11 presents the thermogravimetric curve of the I_2@AC composite tested in a N_2 atmosphere from room temperature to 600 °C. Owing to the low sublimation temperature of I_2, the sharp reduction in mass ratio before 350 °C can be attributed to the volatilization of the I_2 component fixed by the activated carbon, indicating the accurate I_2 content in I_2@AC composite can be determined as 38.67 wt.%. In order to check the electrochemical reaction mechanism of I_2@AC cathode in different electrolytes, the cyclic voltammetry (CV) curves of Zn//I_2@AC batteries in UE and BE were simultaneously implemented. As shown in Figure 4A, there are two pairs of redox peaks for Zn//I_2@AC batteries in UE, respectively representing the I^-/I_0 (1.25 V/1.375 V) and I_0/I^+ (1.7 V/1.75 V) redox couple, which can be determined as 4eZIBs. In contrast, there is only one pair of redox peaks for Zn//I_2@AC batteries in BE, corresponding well to the redox reaction between I^- and I_0 (1.25 V/1.375 V, Figure 4B). Similarly, Figure 4C displays the galvanostatic charge/discharge curves of I_2@AC cathode in different electrolytes within 0.6-1.85 V, exhibiting a single redox plateau in BE and two redox plateaus in UE, which is well consistent with the results of CV curves. Generally, more electron transfer means a higher specific capacity and operating voltage platform, inducing a higher energy density of ZIBs. Profiting from the four-electron transfer reactions of Zn//I_2@AC batteries in UE, I_2@AC cathode in UE delivers high discharge capacity of 187.2 mAh g^{-1} after 250 cycles at the current density of 1 A g^{-1}, which is higher than that in BE [Figure 4D]. It is worth mentioning that the initial higher discharge capacity in BE can be mainly attributed to the serious side reactions of $Zn(AC)_2$-based electrolytes, such as OER and HER. Supplementary Figure 12 compares the cycling performances of urea electrolytes with different concentrations to explain the influence of their concentrations on battery performance. Urea at too low concentrations cannot completely inhibit the hydrolysis of I^+, and urea at too high concentrations leads to excessive viscosity of the electrolyte. Similarly, a high-concentration salt solution not only brings economic impracticality but also reduces the ionic conductivity, resulting in a decline in battery performance [Supplementary Figure 13]. Figure 4E, Supplementary Figure 14 compares the EIS curves of Zn//I2@AC batteries after 50 cycles in different

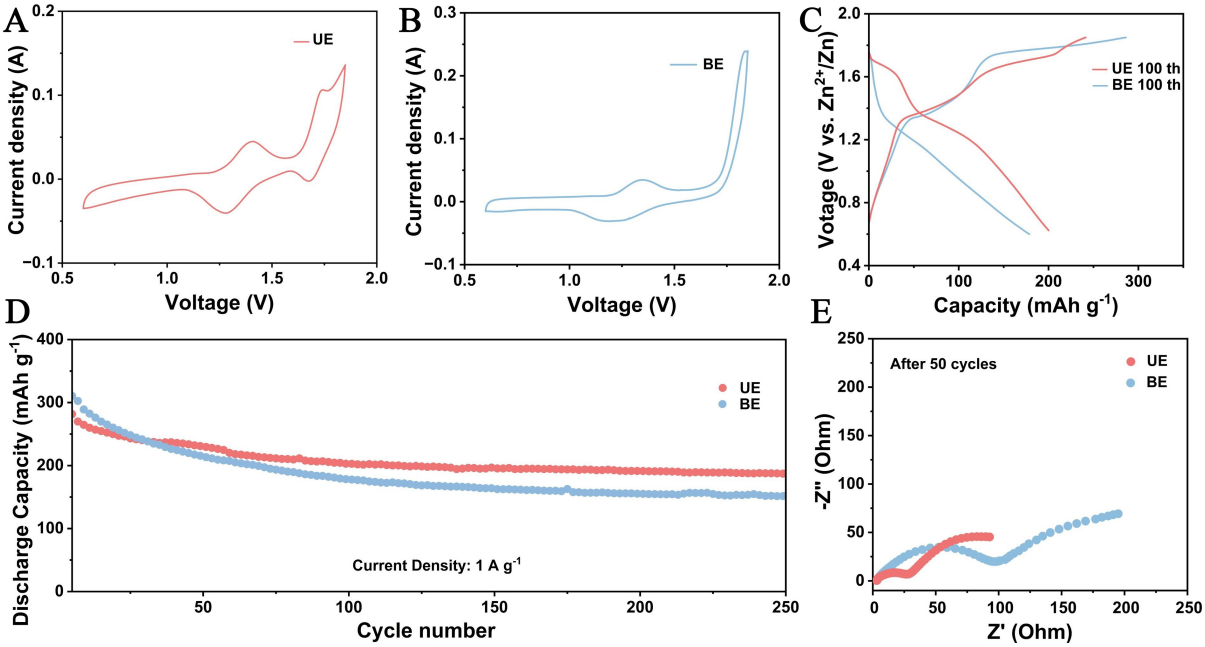

Figure 4. CV curves of I_2@AC cathode in the electrolytes of (A) UE and (B) BE within 0.6-1.85 V at 0.1 mV s^{-1}; (C) The 100th galvanostatic charge and discharge curves of I_2@AC cathode in different electrolytes within 0.6-1.85 V; (D) Cycling performances of Zn//I_2@AC batteries in different electrolytes at the current density of 1 A g^{-1}; (e) Electrochemical impedance spectroscopy curves of Zn//I_2@AC batteries after 50 cycles in different electrolytes. CV: cyclic voltammetry; UE: urea electrolyte; BE: blank electrolyte.

electrolytes, as well as their impedance fitting graphs and equivalent circuit diagrams, to jointly reveal the interfacial charge transfer behavior. Briefly, the semicircle at middle-to-high frequency regions corresponds to the charge transfer impedance (R_{ct}), the smaller radius of Zn//I_2@AC batteries in UE manifests its lower charge-transfer energy barrier, which conduces to promote the interfacial reaction kinetics to some extent.

To disclose the valence changes of I_2@AC cathode in different electrolytes, Supplementary Figures 15 and 16 respectively investigate the high-resolution C 1s and I 3d spectra at different charged/discharged states by XPS technique. Semiquantitatively, compared with the discharged state, the binding energy of I 3d in UE at the fully charged state delivers a more pronounced shift to a higher energy level [Supplementary Figure 16A], which can be illustrated by the oxidation reaction of I_2@AC cathode from I^- to I^+ during the charging process. For the I_2@AC cathode in BE, the shift of I 3d binding energy is relatively flat [Supplementary Figure 16B], thereby suggesting the lower level of valence rise from I^- to I_0[16,40]. Supplementary Figure 17 provides a detailed schematic comparison of solvation structure and action mechanism for I^+ species between UE and BE. In consequence, BE represents the classical hydrogen bonds network, *i.e.*, one H_2O molecule forms four hydrogen bonds and cross-links with each other, and these active H_2O molecules are highly susceptible to hydrogen evolution and oxygen evolution reactions. Meanwhile, the H_2O molecule holds good nucleophilicity, while the I^+ species hold good nucleophilicity, thus leading to the severe hydrolysis reaction within active H_2O and I^+ ions, which seriously degrades the cyclic stability of ZIBs. As a striking contrast, the introduction of urea molecules in UE acts as both a donor and an acceptor of hydrogen bonds, which recombines the hydrogen bonds within the H_2O-H_2O bridges, bundles part of active H_2O molecules, and reduces the electrolyte reactivity of UE. Additionally, the -NH_2 groups in urea molecule also possess superior nucleophilicity, which can compete with H_2O molecules for the existing I^+ ions, form covalent bonds with I^+ ions, and effectively block the hydrolysis reaction of I^+ species, thus realizing durable and stable 4eZIBs.

CONCLUSION

In summary, urea with diamine ligand sites (-NH_2) was introduced into the liquid electrolyte to block the spontaneous hydrolysis reaction of I^+ species and achieve stable 4eZIBs. Based on the spectroscopic characterization results of electrolytes, the urea molecules in UE serve as both donors and acceptors of hydrogen bonds, which effectively reconstructs the hydrogen bond structure, weakens the electrolyte reactivity, and acts as nucleophilic sites to inhibit the hydrolysis of I^+ ions. As expected, the optimized UE electrolyte can not only enlarge the electrochemical stable voltage window, but also realize the coupled redox reactions within $I^-/I_0/I^+$ species. Benefitting from the four-electron transfer reactions in UE, the I_2@AC cathode exhibits a reversible discharge capacity of 187.2 mAh g^{-1} after 250 cycles at 1 A g^{-1}, and this regulation strategy can provide a promising direction to design suitable electrolytes with low salt concentration for high-performance 4eZIBs.

DECLARATIONS

Authors' contributions

Conceived and designed the article: Guo, Q.; Qiu, C.; Li, J.
Carried out electrochemical tests and characterizations: Guo, Q.; Li, F.
Drafted and revised manuscript: Guo, Q.; Qiu, C.; Liu, W.; Tian, X.
Assisted with the data analysis and characterization: Zhang, Y.; Chen, Z.
Supervised the overall project: Liu, W.; Shi, X.
All authors reviewed the results and approved the final version of the manuscript.

Availability of data and materials

The data that support the findings of this study are available from the corresponding author upon reasonable request.

Financial support and sponsorship

The authors thank the National Natural Science Foundation of China (52404316, 52461040, 52474325, and 52274297), Natural Science Foundation of Hainan Province (621RC512 and 524RC475), and Collaborative Innovation Center of Marine Science and Technology of Hainan University (XTCX2022HYC14). Additionally, the authors acknowledge the support for comprehensive characterizations by Pico Election Microscopy Center of Hainan University.

Conflict of Interest

All authors declared that there are no conflicts of interest.

Ethical approval and consent to participate

Not applicable.

Consent for publication

Not applicable.

REFERENCES

1. Chen, M.; Rao, P.; Miao, Z.; et al. Strong metal-support interaction of Pt-based electrocatalysts with transition metal oxides/nitrides/carbides for oxygen reduction reaction. *Microstructures* **2023**, *3*, 2023025. DOI
2. Wan, Y.; Liu, Y.; Chao, D.; Li, W.; Zhao, D. Recent advances in hard carbon anodes with high initial Coulombic efficiency for

sodium-ion batteries. *Nano. Mater. Sci.* **2023**, *5*, 189-201. DOI

3. Geng, X.; Hou, X.; He, X.; Fan, H. J. Challenges and strategies on interphasial regulation for aqueous rechargeable batteries. *Adv. Energy. Mater.* **2024**, *14*, 2304094. DOI
4. Zhong, Y.; Cao, C.; Zhao, L.; Tadé, M. O.; Shao, Z. Optimization of two-dimensional solid-state electrolyte-anode interface by integrating zinc into composite anode with dual-conductive phases. *Green. Carbon.* **2024**, *2*, 94-100. DOI
5. Yang, T.; Niu, Y.; Liu, Q.; Xu, M. Cathode host engineering for non-lithium (Na, K and Mg) sulfur/selenium batteries: a state-of-the-art review. *Nano. Mater. Sci.* **2023**, *5*, 119-40. DOI
6. Khan, Z.; Kumar, D.; Crispin, X. Does water-in-salt electrolyte subdue issues of Zn batteries? *Adv. Mater.* **2023**, *35*, e2300369. DOI PubMed
7. Du, D.; Zeng, L.; Lan, N.; et al. Understanding and mastering multiphysical fields toward dendrite-free aqueous zinc batteries. *Adv. Energy. Mater.* **2024**, *14*, 2403153. DOI
8. Li, H.; Li, S.; Hou, R.; et al. Recent advances in zinc-ion dehydration strategies for optimized Zn-metal batteries. *Chem. Soc. Rev.* **2024**, *53*, 7742-83. DOI
9. Li, D.; Cao, L.; Deng, T.; Liu, S.; Wang, C. Design of a solid electrolyte interphase for aqueous Zn batteries. *Angew. Chem. Int. Ed.* **2021**, *60*, 13035-41. DOI
10. Wu, M.; Wang, X.; Zhang, F.; Xiang, Q.; Li, Y.; Guo, J. Highly reversible and stable Zn metal anodes realized using a trifluoroacetamide electrolyte additive. *Energy. Environ. Sci.* **2024**, *17*, 619-29. DOI
11. Cao, L.; Li, D.; Hu, E.; et al. Solvation structure design for aqueous Zn metal batteries. *J. Am. Chem. Soc.* **2020**, *142*, 21404-9. DOI
12. Zhang, Q.; Ma, Y.; Lu, Y.; et al. Modulating electrolyte structure for ultralow temperature aqueous zinc batteries. *Nat. Commun.* **2020**, *11*, 4463. DOI PubMed PMC
13. Yan, L.; Zhang, S.; Kang, Q.; et al. Iodine conversion chemistry in aqueous batteries: challenges, strategies, and perspectives. *Energy. Storage. Mater.* **2023**, *54*, 339-65. DOI
14. Li, X.; Li, M.; Huang, Z.; et al. Activating the I^0/I^+ redox couple in an aqueous I_2-Zn battery to achieve a high voltage plateau. *Energy. Environ. Sci.* **2021**, *14*, 407-13. DOI
15. Zou, Y.; Liu, T.; Du, Q.; et al. A four-electron Zn-I_2 aqueous battery enabled by reversible $I^-/I_2/I^+$ conversion. *Nat. Commun.* **2021**, *12*, 170. DOI PubMed PMC
16. Wang, M.; Meng, Y.; Sajid, M.; et al. Bidentate coordination structure facilitates high-voltage and high-utilization aqueous Zn-I_2 batteries. *Angew. Chem. Int. Ed.* **2024**, *136*, e202404784. DOI
17. Fialkov, Y. A. Interhalogen compounds as complex-formers. *Russ. Chem. Bull.* **1955**, *3*, 847-55. DOI
18. Whitaker, R.; Ambrose, J.; Hickam, C. Iodine monochloride and iodine trichloride complexes with heterocyclic amines. *J. Inorg. Nucl. Chem.* **1961**, *17*, 254-6. DOI
19. Zong, W.; Li, J.; Zhang, C.; et al. Dynamical Janus interface design for reversible and fast-charging Zinc-iodine battery under extreme operating conditions. *J. Am. Chem. Soc.* **2024**, *146*, 21377-88. DOI
20. Tian, Z.; Guo, W.; Shi, Z.; et al. The role of hydrogen bonding in aqueous batteries: correlating molecular-scale interactions with battery performance. *ACS. Energy. Lett.* **2024**, *9*, 5179-205. DOI
21. Sheng, D.; Liu, X.; Yang, Z.; et al. Hydrogen bond network regulation in electrolyte structure for Zn-based aqueous batteries. *Adv. Funct. Mater.* **2024**, *34*, 2402014. DOI
22. Hao, J.; Zhang, S.; Wu, H.; Yuan, L.; Davey, K.; Qiao, S. Z. Advanced cathodes for aqueous Zn batteries beyond Zn^{2+} intercalation. *Chem. Soc. Rev.* **2024**, *53*, 4312-32. DOI
23. Philbrick, F. A. The hydrolysis of iodine monochloride. *J. Am. Chem. Soc.* **1934**, *56*, 1257-9. DOI
24. Li, D.; Zhu, Y.; Cheng, L.; et al. A MXene modulator enabled high-loading iodine composite cathode for stable and high-energy-density Zn-I_2 battery. *Adv. Energy. Mater.* **2025**, *15*, 2404426. DOI
25. Wang, Z.; Diao, J.; Burrow, J. N.; et al. Urea-modified ternary aqueous electrolyte with tuned intermolecular interactions and confined water activity for high-stability and high-voltage Zinc-ion batteries. *Adv. Funct. Mater.* **2023**, *33*, 2304791. DOI
26. Zhang, R.; Pang, W. K.; Vongsvivut, J.; et al. Weakly solvating aqueous-based electrolyte facilitated by a soft co-solvent for extreme temperature operations of zinc-ion batteries. *Energy. Environ. Sci.* **2024**, *17*, 4569-81. DOI
27. Tao, L.; Lu, X.; Qu, K.; Zeng, Y.; Miller, M. B.; Liu, J. Highly solubilized urea as effective proton donor-acceptors for durable zinc-ion storage beyond single-anion selection criteria. *Small* **2024**, *20*, e2311205. DOI PubMed
28. Tan, H.; Lu, K.; Yuan, G.; et al. Polydentate ligand stabilizes electrolyte and interface layer for anti-corrosion and selective-deposited Zn metal aqueous batteries. *Adv. Funct. Materials.*. DOI
29. Hao, J.; Yuan, L.; Ye, C.; et al. Boosting Zinc electrode reversibility in aqueous electrolytes by using low-cost antisolvents. *Angew. Chem. Int. Ed.* **2021**, *60*, 7366-75. DOI
30. Tan, Y.; Pu, J.; Li, H.; Chao, D. Water molecular activity management towards stable Zn anodes. *Sci. China. Chem.* **2024**, *67*, 4085-97. DOI
31. Zhang, J.; Huang, W.; Li, L.; et al. Nonepitaxial electrodeposition of (002)-textured Zn anode on textureless substrates for dendrite-free and hydrogen evolution-suppressed Zn batteries. *Adv. Mater.* **2023**, *35*, e2300073. DOI
32. Aslam, M. K.; Niu, Y.; Hussain, T.; et al. How to avoid dendrite formation in metal batteries: innovative strategies for dendrite suppression. *Nano. Energy.* **2021**, *86*, 106142. DOI
33. Fu, Q.; Zhang, W.; Liu, X.; et al. Dynamic imine chemistry enables paintable biogel electrolytes to shield on-body zinc-ion batteries

from interfacial interference. *J. Am. Chem. Soc.* **2024**, *146*, 34950-61. DOI

34. Xu, X.; Song, M.; Li, M.; et al. A novel bifunctional Zinc gluconate electrolyte for a stable Zn anode. *Chem. Eng. J.* **2023**, *454*, 140364. DOI
35. Bu, F.; Sun, Z.; Zhou, W.; et al. Reviving Zn^0 dendrites to electroactive Zn^{2+} by mesoporous MXene with active edge sites. *J. Am. Chem. Soc.* **2023**, *145*, 24284-93. DOI
36. Ma, Y.; Ma, Q.; Liu, Y.; et al. Multiphilic-Zn group "adhesion" strategy toward highly stable and reversible zinc anodes. *Energy. Storage. Mater.* **2023**, *63*, 103032. DOI
37. Yan, T.; Liu, S.; Li, J.; et al. Constructing a topologically adaptable solid electrolyte interphase for a highly reversible zinc anode. *ACS. Nano.* **2024**, *18*, 3752-62. DOI
38. Li, W.; Kong, W.; Liu, W.; et al. Ternary eutectic electrolytes attune the electrode/electrolyte interphase layer toward long-life zinc ion batteries. *Energy. Storage. Mater.* **2024**, *65*, 103103. DOI
39. Chen, R.; Zhang, W.; Guan, C.; et al. Rational design of an in-situ polymer-inorganic hybrid solid electrolyte interphase for realising stable Zn metal anode under harsh conditions. *Angew. Chem. Int. Ed.* **2024**, *63*, e202401987. DOI PubMed PMC
40. Li, X.; Wang, Y.; Chen, Z.; et al. Two-electron redox chemistry enabled high-performance iodide-ion conversion battery. *Angew. Chem. Int. Ed.* **2022**, *61*, e202113576. DOI